Title

EFMouse: a Matlab toolbox to model electric fields in the mouse brain

Authors

Ruben Sanchez-Romero[1], Sibel Akyuz[1], Bart Krekelberg[1]

[1] Center for Molecular and Behavioral Neuroscience, Rutgers University, Newark, NJ, 07102, USA

* Corresponding author: ruben.saro@rutgers.edu (R. Sanchez-Romero)

Format: Original research paper

Highlights

- EFMouse is a novel, open-source, Matlab-based electric field simulator for the mouse brain.
- EFMouse quantifies field focality and homogeneity in regions of the Allen Mouse Brain Atlas.
- Focal and strong stimulation can be produced with two or five electrode montages.
- A high-density montage with a lumbar return generates fields perpendicular to the cortical surface.

Abstract

Compared to the rapidly growing literature on transcranial electrical stimulation (tES) in humans, research into the mechanisms underlying neuromodulation by tES using in-vivo animal models is growing but still relatively rare. Such research, however, is key to overcoming experimental limitations in humans and essential to build a detailed understanding of the in-vivo consequences of tES that can ultimately lead to development of targeted and effective therapeutic applications of noninvasive brain stimulation. The sheer difference in scale and geometry between animal models and the human brain contributes to the complexity of designing and interpreting animal studies. Here we extend previous approaches to model intracranial electric fields to generate predictions that can be tested with in-vivo intracranial recordings. Although the toolbox has general applicability and could be used to predict intracranial fields for any tES study using mice, we illustrate its usage by comparing fields in a high-density multi-electrode montage with a more traditional two electrode montage. Our simulations show that both montages can produce strong focal homogeneous electric fields in targeted areas. However, the high-density montage produces a field that is more perpendicular to the visual cortical surface, which is expected to result in larger changes in neuronal excitability.

Keywords: electrical stimulation; electric field modeling; mouse models; high-definition stimulation.

Data/code availability statement: Data and code to reproduce our analyses will be made publicly available upon acceptance of the manuscript (https://github.com/klabhub/EFMouse).

Declaration of interests: The authors have no conflicts of interest to declare.

Author statement:
Ruben Sanchez-Romero: Conceptualization, Methodology, Software, Formal Analysis, Writing-original draft, Writing-review & editing, Visualization.
Sibel Akyuz: Conceptualization, Methodology, Writing-review & editing.
Bart Krekelberg: Conceptualization, Methodology, Software, Writing-review & editing, Supervision, Resources, Funding acquisition.

Funding: Research reported in this publication was supported by the National Institute Of Neurological Disorders And Stroke and the National Institute on Drug Abuse of the National Institutes of Health under Award Number R01NS120289. The content is solely the responsibility of the authors and does not necessarily represent the official views of the National Institutes of Health.

Introduction

Understanding intracranial current flow is an important aspect of harnessing the potential of transcranial current stimulation. Here we build on previous approaches (Thielscher et al., 2015; Huang et al., 2019) with a particular focus on the mouse brain in which our future studies will test model predictions against empirical observations of neural response properties using two-photon imaging. The toolbox has general applicability and could be used to estimate fields for any tES study using mice, but we illustrate its usage here by comparing intracranial fields in a high-density multi-electrode montage with a more traditional two electrode montage.

The reported behavioral effects of transcranial electrical stimulation (tES) with high-definition montages suggest that such electrode arrangements are a promising approach to develop effective stimulation protocols. High-definition montages aim to increase the focality of the induced electric field in targeted areas, and generally use a center-surround arrangement with varying number of electrodes (Dmochowski et al., 2011; Edwards et al., 2013). Studies using high-definition montages for transcranial alternating current (tACS) or direct current (tDCS) stimulation, have reported significant behavioral effects, for example, in motion perception (Helfrich et al., 2014); visuo-spatial working memory and mental rotation (Zhang et al., 2022); feedback guided learning (Reinhart, 2017); and working memory in older adults (Reinhart and Nguyen, 2019). These findings suggest that the focality of the high-definition montages plays a role in the effectiveness of transcranial stimulation. Direct evidence to support such a claim can be found in a small number of studies that directly compare high-definition vs. conventional montages. For instance, (Gözenman and Berryhill, 2016), show a statistical interaction between montage and working memory conditions, and speculate that the difference in behavioral effects could be explained in terms of focality (affecting a region of interest) or diffusivity (affecting a large scale network) of the induced electric field. (See also Hogeveen et al., (2016) and Masina et al., (2021).)

In-vivo intracranial measurements provide the most direct assessment of the nature of intracranial fields caused by transcranial stimulation. Opitz et al., (2016, 2018) and Huang et al., (2017) provide such measurements of electric field magnitudes in humans. While important, such studies with human volunteers are necessarily somewhat limited because recording electrodes are placed based on clinical considerations and not to test the properties of induced electric fields. These limitations are partially addressed by translational work in animal models (Asan et al., 2019; Opitz et al., 2016) and human cadavers (Vöröslakos et al., 2018; Violante et al., 2023), although these come with a different set of caveats (Opitz et al., 2017). Reviews by Beliaeva et al., (2021) and Jackson et al., (2016) provide a list of considerations to better translate electrical stimulation experiments in rodents and non-human primates to humans, for example, differences in brain geometry that determine the flow of electric current, orientation of targeted neuronal columns and placement of stimulation electrodes, organization of functional networks related to targeted behavior, and the need to adjust parameters, such as the injected current, to achieve field magnitudes that could realistically be achieved in human applications.

Given the technical challenges of intracranial field recordings, electric field models provide an important complementary approach to investigate a wide range of different conditions of interest. Alekseichuk et al., (2019) used high-resolution anatomical mesh models to compare electric fields across mouse, monkey, and human brains and Bernabei et al., (2014) used the same anatomical mouse mesh to simulate a montage with one electrode clipped in each ear. These studies primarily reported results at the whole-brain level—emphasizing general similarities and differences between species. Here we build on these approaches by developing a mouse electric field model (EFMouse) specifically for experiments in which the neural consequences of stimulation are measured invasively. This requires a number of refinements in the model: we modeled the skin defects and the craniotomies that are necessary to probe intracranial responses; we

developed an approach that allows the stimulation electrodes to be placed anywhere on the animal's body; and created tools to quantify field properties in arbitrary regions of interest defined by stereotaxic orientations, or in identified regions of the Allen Mouse Brain Atlas. These steps bring us closer to a model that informs questions about target and off-target stimulation, enables the comparison of the relative benefits of different montages, and ultimately predicts specific (neural or behavioral) outcomes in an experiment.

In this paper, we present the considerations and technical solutions that led to EFMouse (Methods) and then illustrate its use by asking a series of questions about a planned experiment in which electrical stimulation is used to target mouse visual cortex and the neural consequences are recorded using two-photon imaging (Results). Researchers can easily adapt EFMouse to their own questions using the Matlab tutorials included in the project repository (https://github.com/klabhub/EFMouse).

Materials and Methods

Mouse mesh

We use the mesh mouse model published by Alekseichuk et al. (2019), which itself is based on images provided by the Digimouse project (Dogdas et al., 2007). In short, the mesh corresponds to one 28 grams normal nude male mouse for which post-mortem isotropic 0.1mm voxel images were acquired (CT, PET and cryosection). The high-resolution mesh provided by Alekseichuk et al., consists of approx., 1M nodes and 5.7M tetrahedra, and segments the mouse whole-body into five broad structures with corresponding conductivity values: gray matter (0.275 siemens per meter, S/m), CSF (1.654 S/m), bone (0.01 S/m), soft tissue (0.465 S/m) and eyeballs (0.5 S/m). We changed the mesh's orientation to left to right (x-axis), posterior to anterior (y-axis), and inferior to superior (z-axis) to match stereotaxic conventions of the Paxinos atlas (Paxinos and Franklin, 2019).

Craniotomy

Measuring neural consequences of stimulation at the single neuron level requires an invasive approach, and therefore a craniotomy. Modeling this included two components. First, to model the removal of the skin, we set the conductivity of the skin tetrahedra above the craniotomy to that of air (2.5e-14 S/m, value taken from ROAST (Huang et al., 2019) (https://github.com/andypotatohy/roast/)). Second, we assumed that CSF would fill the volume of the part of the skull that was removed. To model this, we set the conductivity of the tetrahedra corresponding to the removed skull volume to that of cerebral spinal fluid (CSF).

Electrode placement

Following the same approach as for the craniotomy, we modeled electrodes by changing the conductivity values of existing elements of the tetrahedral mesh to a highly conductive 5.9e7 S/m (value taken from ROAST). Specifically, this included circular electrodes of 1 mm diameter and 0.85 mm depth placed in the skin tetrahedra. For the 4x1 montage we placed four anodes in anterior, posterior, lateral, and medial positions surrounding the craniotomy, and one cathode in the lumbar area of the mouse (**Figure 1A**). We selected 0.2 mA total current based on the experiments of Asan et al., (2020) and Dockery et al., (2011), and distributed this current across the four anodes (+0.5 mA each) while returning all current through the single cathode (-0.2 mA). For the 1x1 montage, we placed an anode anterior to the craniotomy, and a cathode posterior (**Figure 1B**). In the 1x1 montage, the anode received +0.2 mA and the cathode returned -0.2 mA (**Figure 1B**).

Guiding placement

The anatomical resolution of the mesh does not provide detailed landmarks. To improve the placement of instrumentation (e.g., the craniotomy and the electrodes), we manually coregistered volumetric NIfTI files for the Digimouse with the visual areas defined in the Allen atlas (see **Figure 4** for a volume slice example). EFMouse provides a function to map from volumetric coordinates to mesh coordinates. (Digimouse and Allen atlas NIfTI files are provided in the repository.)

Electric field modeling

The finite element method (FEM) solution for the electric field problem described by the mouse, craniotomy, electrodes, conductivities, and injected currents, is based on the ROAST implementation but adjusted to the specifics of our mouse model. In contrast to human optimized tES simulators, our electrodes do not use conductive gel but are inserted directly into the mouse tissue (eg., skin or bone), this is reflected in the definition of the electrode boundary conditions. We solved the FEM electrostatic problem using the open-access solver GetDP (Dular et al., 1998) (https://getdp.info/), keeping the ROAST default parameters. This results in a voltage (V), electric field components in x,y, and z directions (V/m) and an electric field magnitude (V/m) at each node in the mesh.

Relative focality

We defined relative focality as the fraction of nodes in a *reference region* with an electric field magnitude (eMag) greater than the 75% of the 99.9th percentile of the eMag distribution for the *target region*. A low fraction indicates high relative focality, and a large fraction indicates low relative focality. This extends the definition of focality used by Fernandes et al., (2024). High focality indicates that a small number of reference areas have eMag values as high as the ones observed in the target area, suggesting that the montage is able to produce a strong electric field concentrated in the target area. Low focality indicates the opposite, a large number of reference areas with eMag values as high as the target area, suggesting a montage with more diffuse effects.

Direction homogeneity

In-vitro recordings show the importance of the direction of the induced field relative to the orientation of the major axis of the neurons (Bikson et al., 2004; Lafon et al., 2017). Based on such results, a field with small magnitude aligned homogeneously with the neurons could have a bigger influence than a misaligned field with large magnitude. We define direction homogeneity as the magnitude of the mean of the normalized components across all nodes in a given region.

Direction homogeneity is computed as *sqrt*(mean(eX_n)^2 + mean(eY_n)^2 + mean(eZ_n)^2), where eX_n = eX/eMag, is the normalized field component for each node, equivalently for eY_n and eZ_n. We use normalized components since direction homogeneity only quantifies the direction of the field. Also, by using normalized components, direction homogeneity ranges from 0 to 1, with larger values indicating more homogeneity and thus electric field components with a more uniform direction. (As an extreme example, if half of the nodes point to positive x-direction and the other half to negative x-direction, similarly for y and z components, the field direction homogeneity will be equal to zero.) In Results, we report direction homogeneity together with mean normalized x, y and z components.

Implementation

The toolbox was implemented using an object-oriented approach in Matlab R2023a. The code is documented extensively, includes tutorials matching the simulations presented in this paper, and is available at https://github.com/klabhub/EFMouse.

Results

We developed a Matlab toolbox (EFMouse) to simulate intracranial fields in the mouse brain produced by current stimulation. The GitHub repository (https://github.com/klabhub/EFMouse) contains tutorials and tools that allow researchers to ask their own specific questions. Here we illustrate its use by asking a series of questions arising from ongoing experiments investigating the neural consequences of tDCS using two-photon imaging. In these experiments, the goal was to target the left visual cortex of the mouse while recording neural activity using two-photon microscopy. (For similar setups see Monai et al., (2016), Michelson et al., (2019), Dadarlat et al., (2024).)

Our first question was whether a high-density montage provides an advantage over a traditional two-electrode montage. **Figure 1A** shows the high density 4x1 montage, **Figure 1B** the traditional 1x1 montage, both with stimulation electrodes inserted into the skin (red), and a craniotomy representing the removal of skin (green) and bone (yellow) (Methods).

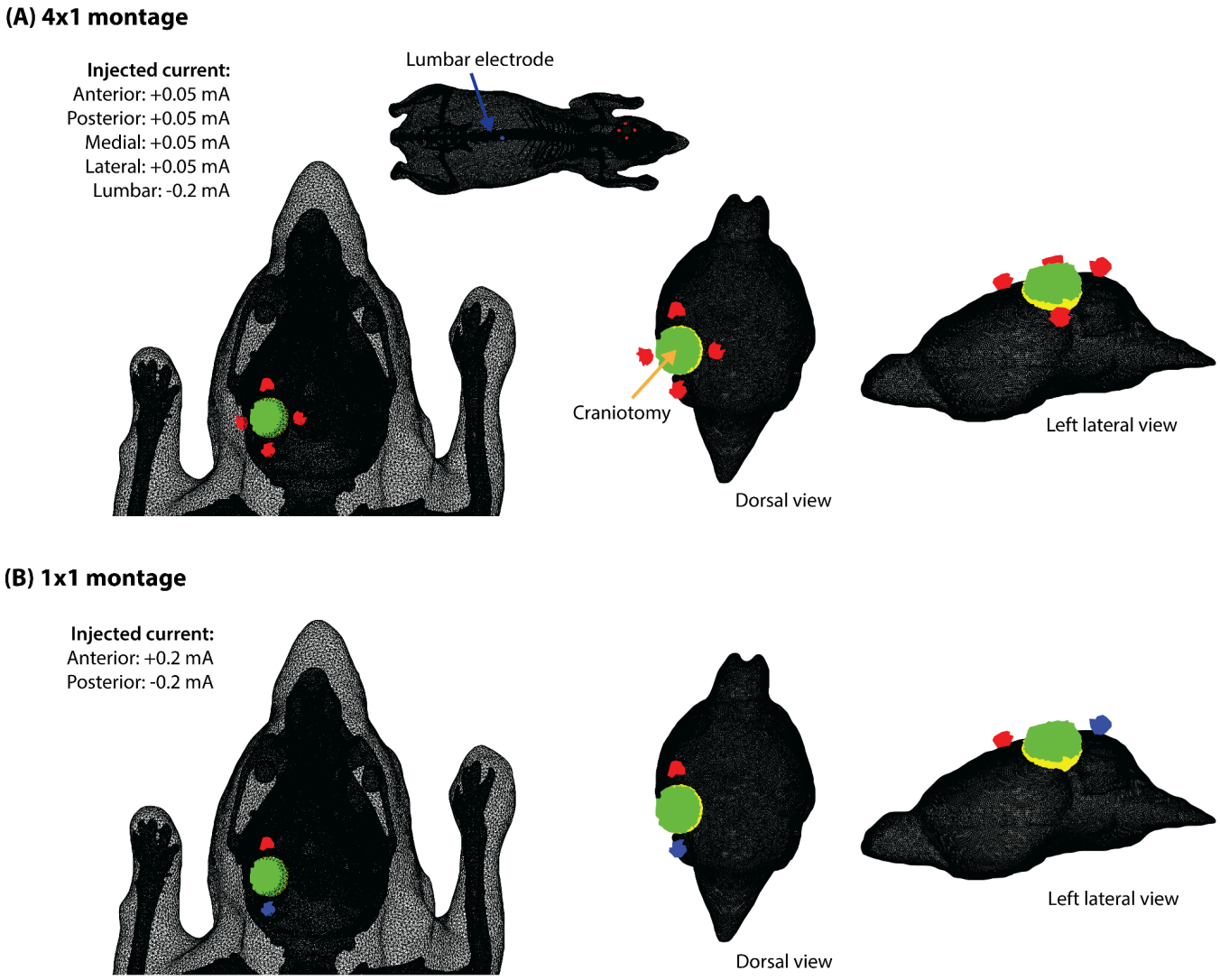

Figure 1. Craniotomy and electric stimulation montage. Visualization in mesh space for (A) 4x1 montage, and (B) 1x1 montage. The montage is represented relative to the mouse skin and bone (left panels) and relative to the mouse brain (right panels). For the craniotomy, skin removal is depicted in green, and underlying bone removal is depicted in yellow, anodes in red, and cathodes in blue.

Whole brain electric field

We start with an analysis of the predicted field at the whole brain level (labeled in the Digimouse/Alekseichuk mesh as “gray matter”, it contains olfactory bulbs, cortex, subcortex, cerebellum and brainstem), to visualize the general spatial patterns of the field across the brain (**Figure 2**). Visual inspection of **Figure 2** suggests that both montages target the left visual cortex, in the sense that the area surrounding craniotomy and electrodes has a higher field magnitude than the contralateral right area. This overall view, however, glosses over some potentially important differences.

Table 1 shows that both montages indeed achieve a similar field magnitude (mean and median). However, the 4x1 montage has a large dorsal to ventral component (negative component in the z direction, eZ mean = -1.66 V/m) and a lateral to medial (positive component in the x direction, eX mean = 1.27 V/m), consistent with the position of the lumbar return electrode (see **Figures 1A**, **2A**). In contrast, the 1x1 montage primarily generates

a tangential field (anterior to posterior; negative component in the y direction, eY mean = -1.67 V/m), consistent with the position of the return electrode (see **Figures 1B**, **2B**). These differences are also reflected in the direction homogeneity measure (Methods), which is 0.83 for the 4x1 montage with mean normalized components (0.51, -0.16, -0.63), indicating more uniform components in the positive x- and negative z-direction. By contrast, the 1x1 montage has a direction homogeneity of 0.72 with (0.31, -0.59, -0.26), indicating a more uniform component in the negative y-direction. (Note that we report results here only for the mouse brain but EFMouse can also produce electric field summary statistics for the rest of the mesh tissues/elements, including soft tissue, bone, CSF, eyeballs, craniotomy and electrodes. See the results/tutorial Matlab notebooks in the repository).

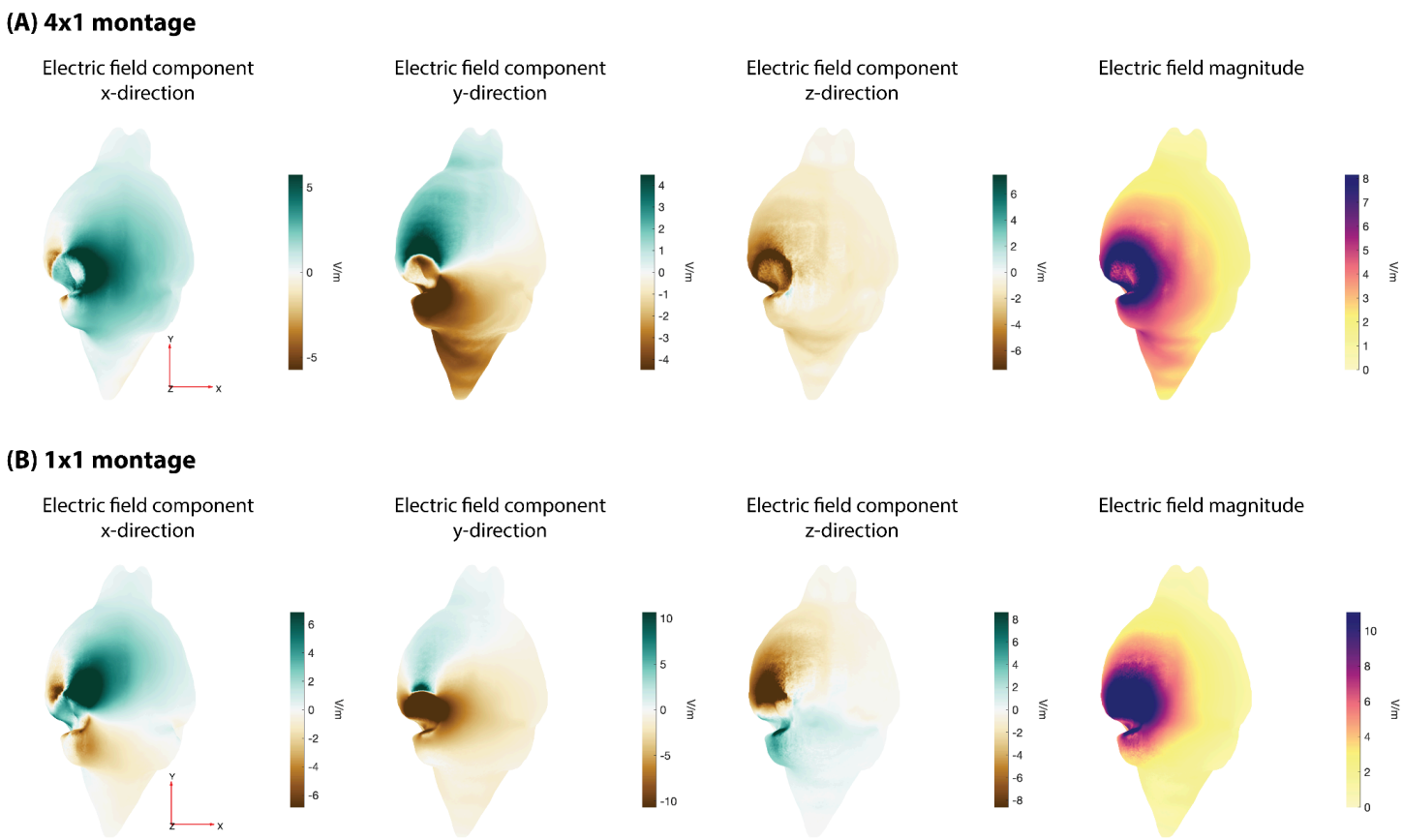

Figure 2. Predicted electric field (V/m) in the whole Digimouse brain. Visualization in mesh space. Results for (A) 4x1 and (B) 1x1 montages. To remove outliers from this visualization, field magnitudes are capped at the 98th percentile.

Table 1. Summary statistics for the predicted electric field (V/m) in the whole Digimouse brain. Results for the x, y and z direction field components (eX, eY and eZ), and for the field magnitude (eMag), for the 4x1 and 1x1 montages.

Whole brain											
	4x1 montage						**1x1 montage**				
	mean	**median**	**std**	**min**	**max**		**mean**	**median**	**std**	**min**	**max**
eX	1.27	0.99	1.15	-5.42	14.53	**eX**	0.79	0.68	1.68	-11.72	26.46
eY	-0.55	-0.31	1.55	-12.78	12.11	**eY**	-1.67	-1.36	2.27	-31.97	19.52
eZ	-1.66	-1.27	1.38	-16.31	2.56	**eZ**	-0.75	-0.40	2.12	-40.61	12.77
eMag	2.64	2.15	1.83	0.21	18.90	**eMag**	2.83	1.99	2.91	0.16	46.88

Region of Interest under the craniotomy

In our planned experiments we will measure neural response properties in the visual cortex below the craniotomy, therefore we are particularly interested in the properties of the predicted electric field in this area. We report results for a box-shaped ROI under the left hemisphere craniotomy (with dimensions x = 1.45 mm, y = 1.24 mm, z = 1 mm) (**Figure 3A**), and for comparison an analogous ROI in the contralateral right region with the same dimensions (**Figure 3B**). Results in **Table 2A** show that for the ROI under the craniotomy, (a) the 1x1 montage produces a stronger mean magnitude; (b) the 4x1 field generates a strong dorsal-to-ventral field (eZ mean = -7.34 V/m), while the field produced by the 1x1 montage is primarily in the tangential anterior-to-posterior y-direction (eY mean = -8.54 V/m). Results in **Table 2B** for the comparison ROI in right visual cortex show that (a) both montages produce weaker fields, and (b) consistent with the whole brain results (**Table 1**), the 4x1 field has preferred -z and +x directions, while, the 1x1 file has a preferred -y direction.

For the 4x1 montage, the ROI under the left craniotomy has a direction homogeneity of 0.99 with mean normalized components (0.38, -0.06, -0.91), while the 1x1 montage has a direction homogeneity of 0.94 with components (0.30, -0.89, 0.02). For the comparison ROI in the right visual cortex, the 4x1 montage has a direction homogeneity of 0.99 with (0.69, -0.42, -0.58), and the 1x1 montage reports 0.98 with (0.11, -0.97, -0.10).

To compute relative focality we consider the ROI under the craniotomy as the *target area*, and the rest of the brain as the *reference area* (Methods). Similarly for the comparison ROI. For the ROI under the craniotomy, the 4x1 montage relative focality was 1.05% (out of 161,805 brain nodes), and for the 1x1 montage it was 1.20% (out of 161,805 nodes). In other words, for both montages, only 1% of the brain outside the target area received a field that was similar to the field inside the target area (Methods). For the comparison ROI in the right visual cortex, the 4x1 montage relative focality was 64.36% (out of 161,805 nodes), and for the 1x1 montage it was 57.22% (out of 161,805 nodes).

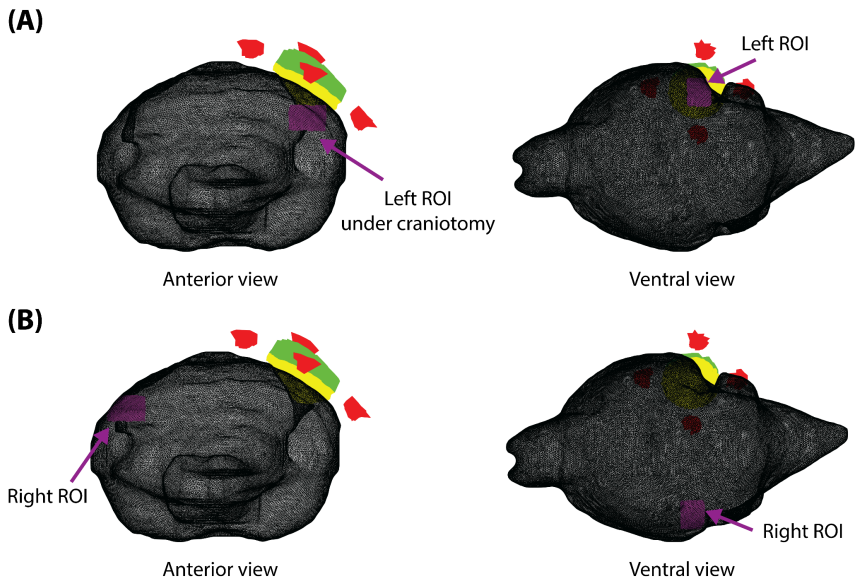

Figure 3. Two box-shaped regions of interest (ROIs) located in the mouse visual cortex. Visualization in mesh space. A target ROI is located under the craniotomy on the left visual cortex. A comparison ROI with analogous dimensions is located on the contralateral right visual cortex. Electrodes and craniotomy for the 4x1 montage only. ROIs are depicted in magenta. (The same ROIs were used for the 1x1 montage.)

Table 2. Summary statistics for the predicted electric field (V/m) for two box-shaped regions of interest (ROIs) located in the mouse visual cortex. Results for (A) ROI under craniotomy in left visual cortex, and (B) analogous ROI in contralateral right visual cortex. Results for the x, y and z direction field components (eX, eY and eZ), and for the field magnitude (eMag), for the 4x1 and 1x1 montages.

(A) ROI under craniotomy in left visual cortex

	4x1 montage						1x1 montage				
	mean	**median**	**std**	**min**	**max**		**mean**	**median**	**std**	**min**	**max**
eX	3.04	2.84	1.14	0.48	8.57	**eX**	2.51	2.57	1.16	-1.49	5.42
eY	-0.47	-0.36	0.95	-4.23	1.62	**eY**	-8.54	-7.98	3.06	-16.53	-2.77
eZ	-7.34	-7.32	1.29	-10.48	-3.54	**eZ**	-0.06	0.44	2.63	-9.18	4.86
eMag	8.09	8.01	1.36	4.45	12.90	**eMag**	9.42	8.67	2.83	5.32	18.62

(B) ROI in right visual cortex

	4x1 montage						1x1 montage				
	mean	**median**	**std**	**min**	**max**		**mean**	**median**	**std**	**min**	**max**
eX	1.28	1.29	0.21	0.71	1.73	**eX**	0.20	0.28	0.29	-0.64	0.72
eY	-0.77	-0.72	0.14	-1.19	-0.53	**eY**	-1.66	-1.62	0.28	-2.43	-1.04
eZ	-1.06	-1.06	0.11	-1.32	-0.74	**eZ**	-0.15	-0.15	0.11	-0.46	0.18
eMag	1.84	1.83	0.20	1.36	2.29	**eMag**	1.70	1.68	0.28	1.11	2.43

Allen atlas visual cortex

The ROI-based analysis above disregards anatomical and functional boundaries. Experimental questions, however, are more often formulated with respect to functionally meaningful regions of interest. To address this, EFMouse can quantify electric field properties using terms defined in the Allen brain atlas. Here, for instance, we computed field measures for the Allen atlas-defined “Visual areas” (**Figure 4**). Results in **Table 3A** for the

left visual cortex are consistent with (and complement) the ROI results from **Table 2A**: (a) the 1x1 montage produces a stronger field than the 4x1; (b) the 4x1 field has preferred -z and +x directions, while the 1x1 has a strong preference for the -y direction. In line with results from **Table 2B**, **Table 3B** shows that for the comparison right visual cortex, both montages produce weaker fields with similar magnitude, and differ in their preferred directions, with the 4x1 field preferring the -z and +x directions, and the 1x1 field the -y direction.

For the Allen atlas left visual cortex, the 4x1 montage reports a direction homogeneity of 0.93 with mean normalized components (0.56, -0.05, -0.74), and the 1x1 montage reports 0.88 with (0.34, -0.79, -0.18). For the comparison right visual cortex, the 4x1 montage reports a direction homogeneity of 0.99 with (0.78, -0.36, -0.48), and the 1x1 montage reports 0.98 with (0.24, -0.95, -0.002).

To compute relative focality we consider the Allen atlas left visual areas as the *target area*, and the whole Allen atlas “Isocortex” (excluding the left visual areas) as the *reference area*. Similarly for the comparison right visual areas. For the left visual cortex, the 4x1 montage relative focality was 0.15% (out of 92,410 Isocortex voxels), and 0.12% (out of 92,410 Isocortex voxels) for the 1x1 montage. For the comparison right visual cortex, the 4x1 montage relative focality was 37.88% (out of 92,457 Isocortex voxels), and for the 1x1 montage it was 48.21% (out of 92,457 Isocortex voxels).

Table 3. Summary statistics for the predicted electric field (V/m) for Allen mouse brain atlas visual cortex. Results for (A) Allen atlas-defined visual cortex in the left hemisphere, and (B) visual cortex in the right hemisphere. Results for the x, y and z direction field components (eX, eY and eZ), and for the field magnitude (eMag), for the 4x1 and 1x1 montages. (Rounding may show some values as zero.)

(A) Allen atlas left visual cortex

	4x1 montage						1x1 montage				
	mean	**median**	**std**	**min**	**max**		**mean**	**median**	**std**	**min**	**max**
eX	4.85	4.94	2.52	-2.19	12.86	**eX**	4.78	3.86	4.68	-5.48	23.52
eY	-0.41	-0.24	2.10	-10.01	7.306	**eY**	-10.72	-10.35	5.22	-28.13	3.35
eZ	-6.38	-6.75	2.53	-13.50	0.00	**eZ**	-3.42	-2.16	5.64	-31.19	10.11
eMag	8.58	8.77	2.87	0.00	16.27	**eMag**	13.91	12.97	6.13	0.01	36.79

(B) Allen atlas right visual cortex

	4x1 montage						1x1 montage				
	mean	**median**	**std**	**min**	**max**		**mean**	**median**	**std**	**min**	**max**
eX	1.71	1.84	0.77	0.00	3.04	**eX**	0.52	0.37	0.48	-0.60	2.276
eY	-0.76	-0.82	0.42	-1.65	0.14	**eY**	-1.95	-2.14	0.84	-3.50	0.00
eZ	-1.04	-1.12	0.46	-1.77	0.00	**eZ**	0.00	-0.06	0.27	-0.76	0.81
eMag	2.17	2.37	0.93	0.00	3.55	**eMag**	2.07	2.24	0.90	0.00	3.54

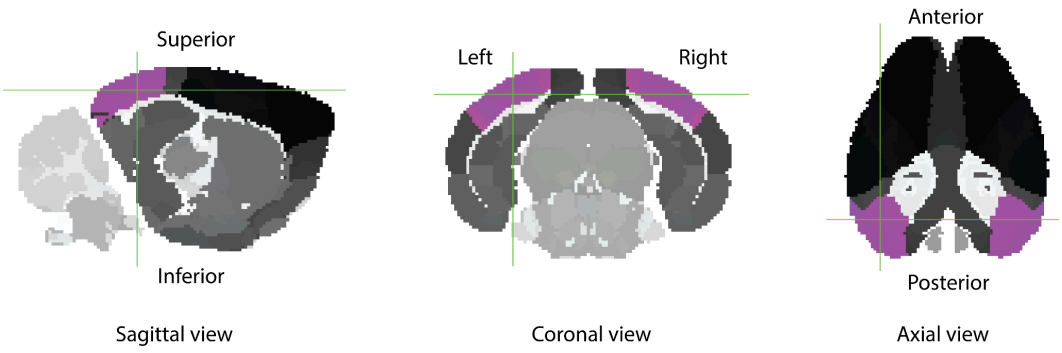

Figure 4. Allen mouse brain atlas visual cortex. The areas labeled “Visual areas” in the Allen atlas are depicted here in magenta. Predicted electric field is analyzed separately for left and right visual cortex (Table 3). (Allen atlas registered to Digimouse volumetric space. Representative slice at voxel (28,85,65) in the Allen atlas NIfTI file provided in the EFMouse repository. Image generated with FSLeyes.)

Discussion

We developed a finite element model of the mouse brain to simulate and analyze electric fields produced by current stimulation. While the model has general applicability, we illustrate its use here by comparing the relative merits of 4x1 vs. 1x1 montages in a planned study investigating the neural consequences of tDCS in mouse visual cortex. We discuss the outcomes and limitations of this specific analysis, as well as some of the limitations and future directions for the EFMouse model.

At the coarse level of electric field magnitude (**Figure 2**, rightmost panels), the fields produced by the 4x1 and 1x1 montages look similar. While such brain surface maps are a common representation of applied fields in studies using tES, our analysis suggests that it is lacking in some important aspects. First, we believe a quantification in terms of target and off-target or control regions (whether defined using coordinate-based ROIs or regions in an atlas) helps understand the specificity of the applied stimulation. Second, this quantification should include some measure of focality that compares target and off-target regions. Third, we found that the 4x1 montage produced a largely radial field (aligned with the principal axis of most neurons in the mouse visual cortical surface), while the 1x1 montage generated a largely tangential field. Because in-vitro recordings suggest that neural outcomes depend on the alignment of the field with the stimulated neurons, quantifying this alignment could help to interpret and compare tES outcomes. These considerations apply equally or potentially even more forcefully to the human brain because its complex geometry and the extensive intersubject variability are expected to generate more inhomogeneous distributions of the magnitude and orientation of tES induced fields.

EFMouse builds on previous work modeling current flow in the brain. We borrowed the mouse anatomical model from Alekseichuk et al. (2019) and the Digimouse project (Dogdas et al., 2007), and the general workflow in the Matlab implementation from ROAST (Huang et al., 2019). We added novel functionality to capture typical surgical approaches in the mouse (e.g., skin removal and cranial recording windows) and the placement of stimulation electrodes anywhere in the animal. These enhancements improve the model’s validity for experiments that include intracranial recording (e.g., Monai et al., (2016); Mishima et al., (2019)), and bone, epidural, or intracranial stimulation (e.g., Ozen et al., (2010); Dadarlat et al., (2024)). In addition, our software adds novel ways to reporting field predictions, including some refined measures of focality and direction homogeneity, and a mapping of simulation results to the Allen Mouse Brain Atlas.

One limitation of EFMouse is that it is based on the one nude male mouse from the Digimouse project (Dogdas et al., 2007). This strain differs from the more commonly used C57BL/6 strain, which was also used for the Allen mouse brain atlas. Although we worked to optimize the coregistration of the Allen atlas to the Digimouse space, this alignment is likely to be imprecise at the level of the finest functional areas (e.g., cortical layers). If a high-resolution mesh for a C57BL/6 mouse becomes available, it could be incorporated into EFMouse, improving the neuroanatomical interpretation of the predicted electric fields.

The current version of EFMouse computes the orientation of the electric field in stereotaxic coordinates. For many cortical areas this can easily be interpreted as radial or tangential orientations (relative to the cortical surface), but this is more complex in some cortical areas with strong curvature, or in subcortical areas (which have not been segmented in the Digimouse mesh). Future work could address this by developing a more detailed segmentation of the whole mouse brain.

In contrast to human studies where anatomical variability can produce substantial differences in effects (Zanto et al., 2021; Preisig and Hervais-Adelman,2022; Hunold et al., 2023), the anatomical homogeneity of inbred mouse strains allows for highly generalizable simulation results across animals. However, when stimulation is combined with intracranial recordings, variability in surgical implants (e.g., location of craniotomies and stimulation electrodes) is a factor that may require individualized models.

In future work, we plan to compare these simulation results with neural data. Such direct comparisons are important to validate the models and critically assess the assumptions underlying the practical or therapeutic application of tES. Ultimately this should allow researchers to design targeted stimulation protocols and effective interventions in humans.

Bibliography

Alekseichuk, I., Mantell, K., Shirinpour, S., & Opitz, A. (2019). Comparative modeling of transcranial magnetic and electric stimulation in mouse, monkey, and human. *Neuroimage*, *194*, 136-148.

Asan, A. S., Gok, S., & Sahin, M. (2019). Electrical fields induced inside the rat brain with skin, skull, and dural placements of the current injection electrode. *PLoS One*, *14*(1), e0203727.

Asan, A. S., Lang, E. J., & Sahin, M. (2020). Entrainment of cerebellar purkinje cells with directional AC electric fields in anesthetized rats. *Brain stimulation*, *13*(6), 1548-1558.

Beliaeva, V., Savvateev, I., Zerbi, V., & Polania, R. (2021). Toward integrative approaches to study the causal role of neural oscillations via transcranial electrical stimulation. *Nature Communications*, *12*(1), 2243.

Bernabei, J. M., Lee, W. H., & Peterchev, A. V. (2014, August). Modeling transcranial electric stimulation in mouse: A high resolution finite element study. In *2014 36th Annual International Conference of the IEEE Engineering in Medicine and Biology Society* (pp. 406-409). IEEE.

Bikson, M., Inoue, M., Akiyama, H., Deans, J. K., Fox, J. E., Miyakawa, H., & Jefferys, J. G. (2004). Effects of uniform extracellular DC electric fields on excitability in rat hippocampal slices in vitro. *The Journal of physiology*, *557*(1), 175-190.

Dadarlat, M. C., Sun, Y. J., & Stryker, M. P. (2024). Activity-dependent recruitment of inhibition and excitation in the awake mammalian cortex during electrical stimulation. *Neuron*, *112*(5), 821-834.

Dmochowski, J. P., Datta, A., Bikson, M., Su, Y., & Parra, L. C. (2011). Optimized multi-electrode stimulation increases focality and intensity at target. *Journal of neural engineering*, *8*(4), 046011.

Dockery, C. A., Liebetanz, D., Birbaumer, N., Malinowska, M., & Wesierska, M. J. (2011). Cumulative benefits of frontal transcranial direct current stimulation on visuospatial working memory training and skill learning in rats. *Neurobiology of learning and memory*, *96*(3), 452-460.

Dogdas, B., Stout, D., Chatziioannou, A. F., & Leahy, R. M. (2007). Digimouse: a 3D whole body mouse atlas from CT and cryosection data. *Physics in Medicine & Biology*, *52*(3), 577.

Dular, P., Geuzaine, C., Henrotte, F., & Legros, W. (1998). A general environment for the treatment of discrete problems and its application to the finite element method. *IEEE transactions on magnetics*, *34*(5), 3395-3398.

Edwards, D., Cortes, M., Datta, A., Minhas, P., Wassermann, E. M., & Bikson, M. (2013). Physiological and modeling evidence for focal transcranial electrical brain stimulation in humans: a basis for high-definition tDCS. *Neuroimage*, *74*, 266-275.

Fernandes, S. R., Callejón-Leblic, M. A., & Ferreira, H. A. (2024). How does the electric field induced by tDCS influence motor-related connectivity? Model-guided perspectives. *Physics in Medicine & Biology*, *69*(5), 055007.

Gözenman, F., & Berryhill, M. E. (2016). Working memory capacity differentially influences responses to tDCS and HD-tDCS in a retro-cue task. *Neuroscience letters*, *629*, 105-109.

Helfrich, R. F., Knepper, H., Nolte, G., Strüber, D., Rach, S., Herrmann, C. S., ... & Engel, A. K. (2014). Selective modulation of interhemispheric functional connectivity by HD-tACS shapes perception. *PLoS biology*, *12*(12), e1002031.

Hogeveen, J., Grafman, J., Aboseria, M., David, A., Bikson, M., & Hauner, K. K. (2016). Effects of high-definition and conventional tDCS on response inhibition. *Brain stimulation*, *9*(5), 720-729.

Huang, Y., Liu, A. A., Lafon, B., Friedman, D., Dayan, M., Wang, X., ... & Parra, L. C. (2017). Measurements and models of electric fields in the in vivo human brain during transcranial electric stimulation. *elife*, *6*, e18834.

Huang, Y., Datta, A., Bikson, M., & Parra, L. C. (2019). Realistic volumetric-approach to simulate transcranial electric stimulation—ROAST—a fully automated open-source pipeline. *Journal of neural engineering*, *16*(5), 056006.

Hunold, A., Haueisen, J., Nees, F., & Moliadze, V. (2023). Review of individualized current flow modeling studies for transcranial electrical stimulation. *Journal of Neuroscience Research*, *101*(4), 405-423.

Jackson, M. P., Rahman, A., Lafon, B., Kronberg, G., Ling, D., Parra, L. C., & Bikson, M. (2016). Animal models of transcranial direct current stimulation: methods and mechanisms. *Clinical Neurophysiology*, *127*(11), 3425-3454.

Lafon, B., Rahman, A., Bikson, M., & Parra, L. C. (2017). Direct current stimulation alters neuronal input/output function. *Brain stimulation*, *10*(1), 36-45.

Masina, F., Arcara, G., Galletti, E., Cinque, I., Gamberini, L., & Mapelli, D. (2021). Neurophysiological and behavioural effects of conventional and high definition tDCS. *Scientific reports*, *11*(1), 7659.

Michelson, N. J., Eles, J. R., Vazquez, A. L., Ludwig, K. A., & Kozai, T. D. (2019). Calcium activation of cortical neurons by continuous electrical stimulation: Frequency dependence, temporal fidelity, and activation density. *Journal of neuroscience research*, *97*(5), 620-638.

Mishima, T., Nagai, T., Yahagi, K., Akther, S., Oe, Y., Monai, H., ... & Hirase, H. (2019). Transcranial direct current stimulation (tDCS) induces adrenergic receptor-dependent microglial morphological changes in mice. *eneuro*, *6*(5).

Monai, H., Ohkura, M., Tanaka, M., Oe, Y., Konno, A., Hirai, H., ... & Hirase, H. (2016). Calcium imaging reveals glial involvement in transcranial direct current stimulation-induced plasticity in mouse brain. *Nature communications*, *7*(1), 11100.

Opitz, A., Falchier, A., Yan, C. G., Yeagle, E. M., Linn, G. S., Megevand, P., ... & Schroeder, C. E. (2016). Spatiotemporal structure of intracranial electric fields induced by transcranial electric stimulation in humans and nonhuman primates. *Scientific reports*, *6*(1), 31236.

Opitz, A., Falchier, A., Linn, G. S., Milham, M. P., & Schroeder, C. E. (2017). Limitations of ex vivo measurements for in vivo neuroscience. *Proceedings of the National Academy of Sciences*, *114*(20), 5243-5246.

Opitz, A., Yeagle, E., Thielscher, A., Schroeder, C., Mehta, A. D., & Milham, M. P. (2018). On the importance of precise electrode placement for targeted transcranial electric stimulation. *Neuroimage*, *181*, 560-567.

Ozen, S., Sirota, A., Belluscio, M. A., Anastassiou, C. A., Stark, E., Koch, C., & Buzsáki, G. (2010). Transcranial electric stimulation entrains cortical neuronal populations in rats. *Journal of Neuroscience*, *30*(34), 11476-11485.

Paxinos, G., & Franklin, K. B. (2019). *Paxinos and Franklin's the mouse brain in stereotaxic coordinates* (5th ed.). Academic press.

Preisig, B. C., & Hervais-Adelman, A. (2022). The predictive value of individual electric field modeling for transcranial alternating current stimulation induced brain modulation. *Frontiers in Cellular Neuroscience*, *16*, 818703.

Reinhart, R. M. (2017). Disruption and rescue of interareal theta phase coupling and adaptive behavior. *Proceedings of the National Academy of Sciences*, *114*(43), 11542-11547.

Reinhart, R. M., & Nguyen, J. A. (2019). Working memory revived in older adults by synchronizing rhythmic brain circuits. *Nature neuroscience*, *22*(5), 820-827.

Thielscher, A., Antunes, A., & Saturnino, G. B. (2015, August). Field modeling for transcranial magnetic stimulation: A useful tool to understand the physiological effects of TMS?. In *2015 37th annual international conference of the IEEE engineering in medicine and biology society (EMBC)* (pp. 222-225). IEEE.

Violante, I. R., Alania, K., Cassarà, A. M., Neufeld, E., Acerbo, E., Carron, R., ... & Grossman, N. (2023). Non-invasive temporal interference electrical stimulation of the human hippocampus. *Nature neuroscience*, *26*(11), 1994-2004.

Vöröslakos, M., Takeuchi, Y., Brinyiczki, K., Zombori, T., Oliva, A., Fernández-Ruiz, A., ... & Berényi, A. (2018). Direct effects of transcranial electric stimulation on brain circuits in rats and humans. *Nature communications*, *9*(1), 483.

Zanto, T. P., Jones, K. T., Ostrand, A. E., Hsu, W. Y., Campusano, R., & Gazzaley, A. (2021). Individual differences in neuroanatomy and neurophysiology predict effects of transcranial alternating current stimulation. *Brain stimulation*, *14*(5), 1317-1329.

Zhang, D. W., Moraidis, A., & Klingberg, T. (2022). Individually tuned theta HD-tACS improves spatial performance. *Brain Stimulation*, *15*(6), 1439-1447.